Molecular Pharmacology Fast Forward. Published on September 12, 2012 as doi:10.1124/mol.112.080184
This article has not been copyedited and formatted. The final version may differ from this version.

MOL #80184

Fe^{2+} block and permeation in $Ca_V3.1$ (α1G) T-type calcium channels. A candidate mechanism for non-tranferrin-mediated Fe^{2+} influx

Kyle V. Lopin, I. Patrick Gray, Carlos A. Obejero-Paz, Frank Thévenod, and Stephen W. Jones

Department of Physiology and Biophysics, Case Western Reserve University, Cleveland, OH 44106, USA (K.V.L., I.P.G., C.A.O., S.W.J.); Universität Witten/Herdecke, ZBAF, Institut für Physiologie & Pathophysiologie, Witten, Germany (F.T.).

Molecular Pharmacology Fast Forward. Published on September 12, 2012 as DOI: 10.1124/mol.112.080184
This article has not been copyedited and formatted. The final version may differ from this version.

Running Title: Fe^{2+} block and permeation in $Ca_V3.1$T-type calcium channels

Corresponding Author:

Stephen W. Jones

Department of Physiology and Biophysics

Case Western Reserve University

Cleveland, OH 44106, USA

Phone: (216) 368-5527

Fax: (216) 368-5586

e-mail: swj@case.edu

33 pages

8 figures

60 references

245 words in Abstract

436 words in Introduction

1281 words in Discussion

Nonstandard abbreviations:

K_D	Dissociation constant
δ	Fractional electrical distance (from the extracellular side)
σ	Surface charge density
τ	Time constant
$P_{O,r}$	Relative P_O
ferrozine	3-(2-Pyridyl)-5,6-diphenyl-1,2,4-triazine-4',4''-disulfonic acid

Molecular Pharmacology Fast Forward. Published on September 12, 2012 as DOI: 10.1124/mol.112.080184
This article has not been copyedited and formatted. The final version may differ from this version.

ABSTRACT

Iron is a biologically essential metal, but excess iron can cause damage to the cardiovascular and nevous systems. We have examined the effects of Fe^{2+}_o on permeation and gating in $Ca_V3.1$ channels, stably transfected in HEK 293 cells, using whole-cell recording. Precautions were taken to maintain iron in the Fe^{2+} state (e. g., extracellular ascorbate). Using instantaneous I-V relations (measured following strong depolarization) to isolate effects on permeation, Fe^{2+}_o rapidly blocked currents with 2 mM Ca^{2+}_o in a voltage-dependent manner, described by a Woodhull model with K_D = 2.5 mM at 0 mV and an apparent electrical distance δ = 0.17. Fe^{2+}_o also shifted activation to more depolarized voltages (by ~10 mV at 1.8 mM Fe^{2+}_o), somewhat more strongly than Ca^{2+}_o or Mg^{2+}_o, consistent with a Gouy-Chapman-Stern model with a surface charge density σ = 1 e^-/98 $Å^2$ and K_{Fe} = 4.5 M^{-1} for Fe^{2+}_o. In the absence of Ca^{2+}_o (and with Na^+_o replaced by tetraethylammonium), Fe^{2+} carried detectable whole-cell inward currents at millimolar concentrations (73 ± 7 pA at -60 mV with 10 mM Fe^{2+}_o). From a 2-site 3-barrier Eyring model for permeation in $Ca_V3.1$, we estimate a transport rate for Fe^{2+} of ~20 ions per second per open channel at -60 mV and pH 7.2, in 1 µM Fe^{2+}_o (with 2 mM Ca^{2+}_o). Since $Ca_V3.1$ exhibits a significant 'window current' in that voltage range (P_O ~1%), $Ca_V3.1$ channels are a likely pathway for Fe^{2+} entry into cells, at clinically relevant concentrations of Fe^{2+}_o.

Molecular Pharmacology Fast Forward. Published on September 12, 2012 as DOI: 10.1124/mol.112.080184
This article has not been copyedited and formatted. The final version may differ from this version.

Introduction

Iron enters cells not only via the well-characterized transferrin receptor-endocytosis pathway for ferric iron, but also the ill-defined non-transferrin bound iron (NTBI) mechanism for both ferric and ferrous iron entry (Anderson and Vulpe, 2009). Candidate mechanisms for NTBI include the divalent metal-ion transporter DMT1, Zip14 (Liuzzi et al., 2006), the non-selective TRPC6 channel (Mwanjewe and Grover, 2004), and voltage gated calcium channels. Both L-type (Oudit et al., 2003; Tsushima et al., 1999) and T-type (Kumfu et al., 2011) calcium channels have been implicated in Fe^{2+} uptake using selective blockers. Currents carried by Fe^{2+} have been recorded electrophysiologically for L-channels (Tsushima et al., 1999) but not T-channels.

Iron overload is typically caused by excess dietary absorption of iron in genetic hemochromatosis (Clark et al., 2010) or repeated blood transfusions when red blood cells are broken down and the heme-bound iron is released (Kwiatkowski, 2011). Plasma NTBI can reach ~5 μM (Loreal et al., 2000). NTBI is highly reactive and can cause the formation of damaging free radicals. Excess iron accumulates mainly in the liver and the heart (Andrews, 1999). In myocardial cells, iron overload affects cellular structure (Iancu et al., 1987), gene expression (Parkes et al., 2000), Ca^{2+} handling (Kim et al., 1995), and ion channel properties (Kuryshev et al., 1999). Because $Ca_v3.1$ channels are widely expressed in excitable and nonexcitable cells including brain, ovary, placenta, heart, liver and vascular smooth muscle (Perez-Reyes, 2003; Rodman et al., 2005; Yunker and McEnery, 2003) understanding the mechanism of Fe^{2+} transport by these channels is necessary to understand their role in organ damage in conditions associated with iron overload.

Besides a role as pore blocker and permeant ion (Tsushima et al., 1999; Winegar et al., 1991), Fe^{2+} might have significant effects on channel gating as is the case for other divalent cations (Elinder and Arhem, 2003). Gating changes induced by divalent cations

Molecular Pharmacology Fast Forward. Published on September 12, 2012 as DOI: 10.1124/mol.112.080184
This article has not been copyedited and formatted. The final version may differ from this version.

may rise from pore occupancy, allosteric effects of binding to sites outside the pore (Beedle et al., 2002; Kang et al., 2005; Traboulsie et al., 2007), or by screening or binding to surface charge (Zhou and Jones, 1995).

We find that Fe^{2+} blocks currents carried by Ca^{2+} or Ba^{2+} by voltage-dependent block within the pore. Fe^{2+} also permeates, less well than Ca^{2+} or Ba^{2+}. Effects of Fe^{2+} on gating are consistent with a surface charge mechanism, where Fe^{2+} both screens and binds to surface charge. The effects of Fe^{2+} to block and shift gating would be minimal at clinically observed concentrations of Fe^{2+}. However, the estimated rates of Fe^{2+} permeation suggest that $Ca_V3.1$ may be a significant source of Fe^{2+} entry into cells even at the resting potential.

Molecular Pharmacology Fast Forward. Published on September 12, 2012 as DOI: 10.1124/mol.112.080184
This article has not been copyedited and formatted. The final version may differ from this version.

Materials and Methods

Electrophysiology. Patch clamp experiments were performed in the whole-cell configuration using HEK 293 cells stably transfected with $Ca_V3.1$ (α1G) calcium channels, as described (Khan et al., 2008). Electrodes were made from borosilicate glass, with open pipet resistances of 1.8-2.3 MΩ, and access resistances of 5 ± 1 MΩ before compensation (80%). Currents were digitally sampled at 50 kHz after 10 kHz analog filtering using an Axopatch 200 amplifier and pClamp 8.2 software. Leak and capacitative currents were subtracted online using a P/-4 protocol. Experiments were performed at room temperature (~22 ^{o}C).

We evaluated the effect of Fe^{2+} using two basic voltage protocols, IV (direct depolarization to a range of voltages) and IIV (preactivating channels by strong, brief depolarization, followed by steps to a range of voltages) (Figs. 1-2). Assuming effects of Fe^{2+} are effectively instantaneous (as we conclude below), this approach allows separation of effects on permeation vs. gating (Hodgkin and Huxley, 1952; Khan et al., 2008; Lopin et al., 2012; Obejero-Paz et al., 2008; Serrano et al., 1999). Currents measured immediately following repolarization with the IIV protocol (Fig. 1A) should be directly proportional to the current through a single open channel. Thus, effects of Fe^{2+} on the IIV relationship should reflect inhibition of current through open channels. Effects on the IV relationship, in contrast, reflect the net effect of the ion both on permeation and on gating.

Standard recording solutions. The intracellular solution contained (in mM) 2 $CaCl_2$, 1 $MgCl_2$, 120 NaCl, 10 HEPES, 4 MgATP, and 11 EGTA, adjusted to pH 7.2 with NaOH (total Na^+ 145 mM, calculated free Ca^{2+} 70 nM). The normal extracellular solution contained 2 $CaCl_2$, 128 NaCl, 5 ascorbic acid, 10 glucose, 20 HEPES, adjusted to pH 7.2 with NaOH (total Na^+ 145 mM). When noted, $CaCl_2$ was replaced by $BaCl_2$.

Molecular Pharmacology Fast Forward. Published on September 12, 2012 as DOI: 10.1124/mol.112.080184
This article has not been copyedited and formatted. The final version may differ from this version.

Extracellular solutions containing Fe^{2+}. Extreme care must be taken to maintain iron in the soluble Fe^{2+} state. To do this $FeCl_2$ was added to the solution only after cells were patched and control currents were being recorded to reduce the amount of time Fe^{2+} could oxidize. Solutions were made 1-2 minutes before they were applied to the cells and were used within the 6 minutes of being made. Fe^{2+} was added to the final desired concentration from a 200 mM stock solution of $FeCl_2 \cdot 4\ H_2O$ in 1% HCl (v/v). Each solution was measured for free Fe^{2+} using the ferrozine method (Dorey et al., 1993; Viollier et al., 2000) while the electrophysiological experiments were being performed. To this end a sample of the extracellular solution was diluted to a final concentration of 100 µM Fe^{2+} with a solution containing the same components (except $FeCl_2$), or a solution containing 5 mM ascorbate (pH 3.3) to reduce all iron forms. 0.75 ml of those samples were mixed with the same volume of 2 mM ferrozine, and absorbance was measured (at 562 nm) in a Beckman DU640B spectrophotometer. Standards in the range from 10 µM and 100 µM Fe^{2+} were prepared by dilution of a stock solution of 20 mM $FeCl_2 \cdot 4\ H_2O$, with a final concentration of 5 mM ascorbic acid. Measured free Fe^{2+} concentrations ranged from 28 – 95% of the nominal value. Throughout this paper, the values for Fe^{2+} concentration are the actual values measured by this procedure.

For experiments examining block by Fe^{2+}, Fe^{2+} was added to the normal extracellular solutions (2 mM Ca^{2+} or 2 mM Ba^{2+}). To investigate whether $Ca_V3.1$ currents allow Fe^{2+} influx, we designed extracellular solutions where Fe^{2+} was the only charge carrier. To this end extracellular NaCl was replaced by TEA-Cl, Ca^{2+} by Fe^{2+}, and solutions were maintained at pH 7.0 to reduce the rate of iron oxidation. A pH of 6.8 – 7.05 measured at the end of the experiment was considered acceptable. A control solution containing 2 mM Ca^{2+} was applied to the cell before and after the test solution.

Since inward currents were small with Fe^{2+}, we performed experiments to evaluate the contribution of gating currents, using an extracellular solution containing (mM) 140 NaCl, 2 $CdCl_2$, and 1 mM $LaCl_3$.

Molecular Pharmacology Fast Forward. Published on September 12, 2012 as DOI: 10.1124/mol.112.080184
This article has not been copyedited and formatted. The final version may differ from this version.

Data Analysis. Most methods were as described (Lopin et al., 2012). Throughout the paper, data are shown as mean ± sem. We used the paired t-test implemented in Origin 7.0 (OriginLab corporation) to assess differences between means when controls were from the same cell. We used one way ANOVA to investigate differences between means from different groups. A two tailed $p<0.05$ was considered statistically significant.

Fe^{2+} block. The voltage dependence of block by Fe^{2+} was described by a model that assumes that Fe^{2+} binds within the electrical field of the membrane, with Fe^{2+} entry and exit exclusively from the extracellular solution (Woodhull, 1973)

$$f = 1/\left\{1+\left[Fe^{2+}\right]/\left(K_{D,0}e^{\frac{z\delta FV}{RT}}\right)\right\} \quad (1)$$

where f is the fraction of peak tail current remaining in the presence of Fe^{2+}, and $K_{D,0}$ is the K_D at 0 mV.

Permeation model. The classical 2-site 3-barrier model of channel permeation (2S3B) (Almers and McCleskey, 1984; Hess and Tsien, 1984), was extended to Fe^{2+}, as for Cd^{2+} (Lopin et al., 2010; Lopin et al., 2012). In brief, parameters for the energy profile of Fe^{2+} were chosen that minimized the sum of absolute error to currents recorded due to Fe^{2+} block and permeation. The parameters for Ca^{2+}, Ba^{2+}, Mg^{2+}, and Na^{+} were fixed to the parameters from Lopin et al. (2010) where they were fit to a wide range of ionic conditions. The minimization procedure produced multiple parameters sets with similar errors (within 15%), all with qualitatively similar currents and energy profiles (all energy parameters varied in a 1 kT range across parameter sets). Because we use the model to predict Fe^{2+} transport rates we chose the parameter set that best fit the currents carried by Fe^{2+}. All other parameter sets predicted Fe^{2+} currents larger than were observed. They also predicted Fe^{2+} transport rates up to twice as large as the parameter set chosen in this paper.

Molecular Pharmacology Fast Forward. Published on September 12, 2012 as DOI: 10.1124/mol.112.080184
This article has not been copyedited and formatted. The final version may differ from this version.

Because control currents in Fe^{2+} permeation experiments were significantly larger than controls in experiments from Khan et al. (2008), we assumed 18000 channels per cell as opposed to 8000. We expect that Fe^{2+} currents are minimally affected by the 0.2 pH unit difference between solutions. Because it was not always possible to record control currents after the test solution we used the first control for normalization, a procedure that will underestimate the iron currents in the presence of current run-down.

Gating. To investigate the effect of Fe^{2+} on channel activation we fitted simultaneously relative open probability ($P_{O,R}$) measured in controls and Fe^{2+} to a fourth-power Boltzmann function

$$Po_R(V) = \left(\frac{1}{1 + e^{\left(\frac{-(V-(V_{0.5} - \delta \cdot \Delta_{V\,0.5}))}{k} \right)}} \right)^4 \qquad (2)$$

where $V_{0.5}$ is the half point of activation of each individual voltage sensor, *k* is the voltage sensitivity, and $\Delta_{V0.5}$ is the shift in $V_{0.5}$ induced by Fe^{2+} and δ is the Kronecker deltafunction where it takes the value of 1 for Fe^{2+} and 0 for controls.

The effect of Fe^{2+} on the rate of channel opening was addressed indirectly studying changes in the time to peak (TP). To this end we simultaneously fitted data from controls and Fe^{2+} to equation 4

$$TP(V) = e^{\left(-\left(V-(V_{1-TP_\infty} - a \cdot \Delta_{V_{1-TP_\infty}})\right)/k\right)} + TP_\infty \qquad (3)$$

where $V_{1\text{-}TP\infty}$ is the voltage at which the time to peak is equal to one minus the asymptotic value of TP (TP_∞), *k* is the voltage sensitivity and $\Delta_{V1\text{-}TP\infty}$ is the shift along the voltage axis.

The effect of Fe^{2+} on the closing rate was investigated fitting simultaneously deactivating time constants between -70 and -120 mV to equation 4

Molecular Pharmacology Fast Forward. Published on September 12, 2012 as DOI: 10.1124/mol.112.080184
This article has not been copyedited and formatted. The final version may differ from this version.

$$\tau(V) = e^{\left(\ln(2)+\frac{(V-(V_{\tau 2ms}-a\cdot\Delta V_{\tau 2m}))}{k}\right)} \quad (4)$$

where $V_{\tau 2ms}$ is the voltage where the time constant equals 2 ms. $\Delta V_{\tau 2ms}$ is the displacement induced by Fe^{2+} along the voltage axis, and *k* is the slope factor.

Gating shifts were calculated using the Minerror procedure (Mathcad) to calculate the values of σ_t and K_{Fe} that minimize χ^2 for $\Delta_{V0.5,}$ $\Delta_{V1\text{-}TP\infty,}$ and $\Delta V_{\tau 2ms}$.

$^{59}Fe^{2+}$ kinetic transport studies. For cellular $^{59}Fe^{2+}$ uptake, $^{59}Fe^{2+}$ was generated from $^{59}FeCl_3$ (specific activity >5Ci(185GBq)/g $FeCl_3$ in 0.5M HCl; Perkin-Elmer, Rodgau, Germany) as described elsewhere (Garrick et al., 2006). $^{59}Fe^{2+}$ uptake (18.5 kBq/ml $^{59}FeCl_2$ in 200-400 µM $FeSO_4$) was performed in confluent monolayers of HEK293 cells or HEK293-$Ca_V3.1$, with or without 25 µM NNC 55-0396, a selective inhibitor of T-type calcium channels (Huang et al., 2004). Monolayers were washed with 2 mM desferrioxamine mesylate, solubilized in 1 N NaOH and cellular radioactivity was measured in a γ-counter.

Molecular Pharmacology Fast Forward. Published on September 12, 2012 as DOI: 10.1124/mol.112.080184
This article has not been copyedited and formatted. The final version may differ from this version.

Results

Effects of Fe^{2+} on permeation. Extracellular application of Fe^{2+} reversibly inhibited currents through $Ca_V3.1$ channels evaluated using the IIV protocol (Fig. 1A). In these ionic conditions (2 mM Ca^{2+}_o and 145 mM $Na^{+}_{i,o}$), $Ca_V3.1$ channels exhibited inward currents carried mostly by Ca^{2+} and outward currents carried by Na^{+}. Note that the inward tail currents in Fe^{2+} were smaller and faster. Peak tail currents were reduced immediately after repolarization, suggesting that Fe^{2+} reached steady-state block rapidly. Block was concentration- and voltage-dependent, with strong inhibition at negative voltages, but little effect on outward currents (Fig. 1B). Fe^{2+} had no clear effect on the reversal potential (Fig. 1C). The voltage dependence of block is best illustrated by chord conductances, especially around the reversal potential (Fig. 1D). The fractional inhibition, measured from chord conductances, was well described by a Woodhull (1973) model (Fig. 1E), suggesting negligible relief of block by hyperpolarization. The data were fitted best with K_D = 2.5 mM at 0 mV, and electrical distance δ = 0.17.

Effects of Fe^{2+} on gating. Fe^{2+} also inhibited currents examined with the IV protocol, evoking currents by direct depolarizations from the holding potential (Fig. 2A). The peak current at each voltage is shown in Fig. 2B, on an expanded scale in Fig. 2C, and as chord conductances in Fig. 2D. With this protocol, inhibition by Fe^{2+} was also voltage-dependent, stronger at more negative voltages, and the voltage producing peak inward current was shifted to more positive voltages (Fig. 2C). Inhibition of peak current could also be described by a Woodhull (1973) model, with K_D = 1.4 mM at 0 mV and δ = 0.33.

Why does the effect of Fe^{2+} appear to be more potent and more voltage-dependent with the IV protocol? The currents recorded in that manner are affected not only by permeation (e. g., channel block), but also by gating (e. g., surface charge effects of Fe^{2+}).

Molecular Pharmacology Fast Forward. Published on September 12, 2012 as DOI: 10.1124/mol.112.080184
This article has not been copyedited and formatted. The final version may differ from this version.

We examined the effects of Fe^{2+} on activation by three measures: effects on the time course of channel activation (Fig. 3A) and deactivation (Fig. 3B), and on the voltage-dependence of peak activation (Fig. 3C). Activation curves were measured as the relative open probability ($P_{O,r}$), calculated as the ratio of peak current from the IV protocol divided by the current at that same voltage from the IIV protocol (Fig. 3C) (Khan et al., 2008; Serrano et al., 1999). This is a more accurate reflection of channel open probability than the more commonly used chord conductance, since the open channel conductance is not constant with voltage (Fig. 1D), so the chord conductances measured with the IV protocol (Fig. 2D) are not pure measures of channel activation (Khan et al., 2008). All three measures of the voltage-dependence of channel gating were affected by Fe^{2+} in a similar manner (Fig. 3D), demonstrating positive shifts along the voltage axis with Fe^{2+}. It is noteworthy that Fe^{2+} did not affect the limiting rates for channel activation (Fig. 3A) or inactivation (Fig. 3B) at strongly depolarized voltages.

Qualitatively, the observed voltage shifts were as expected from a surface charge mechanism, where cations screen a negative surface charge on the extracellular side. Quantitatively, the effect was approximately twice as large as previously observed for Ca^{2+}, Ba^{2+}, and Mg^{2+} (Khan et al., 2008; dashed curve in Fig. 3D). Since simple charge screening (Gouy-Chapman theory) assumes all divalent cations are equivalent, we considered the possibility that Fe^{2+} can bind to the surface charge, as well as screening it (Gouy-Chapman-Stern theory), as observed for Cd^{2+} (Lopin et al., 2012). Fig. 3D demonstrates that the data can be described well by the same surface charge density previously determined for effects of Ca^{2+}, Ba^{2+}, and Mg^{2+} (σ = 1 e^-/98 $Å^2$, Khan et al. 2008), but allowing binding of $Fe^{2+}{}_o$ to the surface charge with K_{Fe} = 4.5 M^{-1}.

Effects of Fe^{2+} with 2 mM Ba^{2+}. $Ca_V3.1$ calcium channels are selective for Ca^{2+} over Ba^{2+} by the classical criterion of permeability ratios, reflecting a more positive reversal potential with Ca^{2+}, indicating greater selectivity vs. monovalent cations (Serrano et al., 2000). Correspondingly, di- and trivalent cations block more rapidly

Molecular Pharmacology Fast Forward. Published on September 12, 2012 as DOI: 10.1124/mol.112.080184
This article has not been copyedited and formatted. The final version may differ from this version.

and/or strongly when Ba^{2+} is the charge carrier, reflecting stronger competition vs. the less permeant Ba^{2+} ion (Mg^{2+}, Serrano et al., 2000; Ni^{2+}, Obejero-Paz et al., 2008; Y^{3+}, Obejero-Paz et al., 2005; Cd^{2+}, Lopin et al. 2012). That was also observed for Fe^{2+} (Figs. 4-5). 0.13 mM Fe^{2+} blocked strongly at hyperpolarized voltages, using either the IIV (Figs. 4A, 5A) or IV protocols (Figs. 4B, 5C). Inhibition measured from chord conductances, using the IIV protocol, was described by a Woodhull model with K_D = 0.33 mM at 0 mV and $\delta = 0.21$ (Fig. 5B). Block was slightly overestimated by the model at the most negative voltages, suggesting relief of block by exit of Fe^{2+} into the cell. That low concentration of Fe^{2+} had minimal effect on channel activation (Fig. 5D). The activation curve was shifted by +2.8 ± 1.0 mV, and time constants for activation and deactivation by 2.9 ± 0.5 mV and -1.0 ± 1.6 mV respectively.

Permeation by Fe^{2+}. When extracellular Ca^{2+} and Na^{+} were replaced by Fe^{2+} and TEA (respectively), inward currents were small but clearly detectable (Fig. 6). Currents were larger in 9 mM vs. 1 mM Fe^{2+} (Fig. 6C), as expected for permeation by Fe^{2+}. The chord conductance in 9 mM Fe^{2+} was 1.5 ± 0.2 -fold larger than in 1 mM Fe^{2+}, averaged from -150 to -50 mV ($p < 0.01$).

An alternative interpretation is that the inward currents observed in Fe^{2+} might be 'off' gating currents. To evaluate that possibility, we compared the integrated tail current amplitudes to gating currents, isolated using a combination of 0.1 mM La^{3+}_o and 2 mM Cd^{2+}_o to block ionic currents (Fig. 7). The insets in Fig. 7A show that the inward currents were larger in Fe^{2+}_o. Quantitatively, the integrated Fe^{2+} tail current greatly exceeded the gating currents at voltages where tail currents were relatively large and slowly decaying (Fig. 7B). The amplitude of the integrated tail current increased with $[Fe^{2+}]_o$ (Fig. 7C). There was considerable scatter in the data, presumably reflecting cell-cell variation in channel expression levels, so the apparent K_D of 4.7 mM for saturation of current with Fe^{2+}_o should be considered a rough estimate.

Molecular Pharmacology Fast Forward. Published on September 12, 2012 as DOI: 10.1124/mol.112.080184
This article has not been copyedited and formatted. The final version may differ from this version.

Reversal potentials were less positive in Fe^{2+} than in Ca^{2+} (Fig. 6C), -26.1 ± 4.7 mV (n=4) in 1.1 mM Fe^{2+}, and -9.0 ± 3.7 mV (n=5) in 8.9 mM Fe^{2+}. Those values correspond to permeability ratios P_{Fe}/P_{Na} = 16 or 5, respectively. That compares to P_{Ca}/P_{Na} = 87 and P_{Ba}/P_{Na} = 44 (Khan et al., 2008), and imply P_{Fe}/P_{Ca} = 0.06-0.18.

Incubation studies with $^{59}Fe^{2+}$ were performed and showed a trend towards increased Fe^{2+} uptake by Ca_v 3.1 channels but were inconclusive due to large background uptake of Fe^{2+} and increased cell death (data not shown).

Model for Fe^{2+} permeation and block. We fitted the data on Fe^{2+} permeation and block to a 2-site 3-barrier (2S3B) Eyring rate theory model (Almers and McCleskey, 1984). The fit of the model to the data is shown for Fe^{2+} permeation (Fig. 8B), and for block of current carried by Ca^{2+}_o (Fig. 8C) or Ba^{2+}_o (Fig. 8D).

We used the model to estimate the extent of Fe^{2+} permeation at concentrations more relevant to physiological or pathophysiological conditions (Fig. 8E-F). Simulated addition of 1-10 μM Fe^{2+} (to extracellular solutions also containing 2 mM Ca^{2+}_o) yielded predicted Fe^{2+} influx at rates up to several hundred ions per second through a single open channel (Fig. 8E). The mechanism of Fe^{2+} permeation predicted by the model is similar to the permeation of Ca^{2+}, with quantitative differences. Both ions seem to get into the pore and bind to the first site similarly but Fe^{2+} is slower to move over to the second site, binds less tightly to second site, and the energy barrier to Fe^{2+} exit from the pore is higher.

$Ca_V3.1$ channels inactivate rapidly and strongly, but inactivation is incomplete, with 1-2% of channels remaining open even after 0.3 sec, 20× the time constant for inactivation (Serrano et al., 1999). This produces a 'window current' that can potentially allow maintained entry of divalent cations into the cell even near the resting potential. When the 2S3B model for permeation was combined with the Serrano et al. (1999) model for gating of $Ca_V3.1$, the predicted steady-state Fe^{2+} influx peaked at 6 ions/sec near -60

Molecular Pharmacology Fast Forward. Published on September 12, 2012 as DOI: 10.1124/mol.112.080184
This article has not been copyedited and formatted. The final version may differ from this version.

mV, in 10 μM Fe^{2+}_o (Fig. 8F). Correction for slow inactivation would lower these values by ~35% (Hering et al., 2004).

Molecular Pharmacology Fast Forward. Published on September 12, 2012 as DOI: 10.1124/mol.112.080184
This article has not been copyedited and formatted. The final version may differ from this version.

Discussion

We conclude that Fe^{2+} affects currents through $Ca_V3.1$ channels by three mechanisms: block of the open pore by Fe^{2+}, shifts in channel activation, and permeation by Fe^{2+}. Fe^{2+} permeates $Ca_V3.1$ pores poorly, compared to Ca^{2+} or Ba^{2+} or even Cd^{2+} (Lopin et al., 2012), but the estimated rate of Fe^{2+} entry suggests that $Ca_V3.1$ is a strong candidate for Fe^{2+} influx in conditions where free $Fe^{2+}{}_o$ is present at micromolar concentrations. We discuss first the biophysical mechanisms of Fe^{2+} interaction with calcium channels, and then the potential implications for iron overload.

Block by Fe^{2+}. The effect of Fe^{2+} on the IIV relationship is consistent with block by occupancy of the pore, presumably at the 'selectivity filter' responsible for selectivity for Ca^{2+} and other di- and trivalent cations. First, block is voltage-dependent, well approximated by a Woodhull (1973) model assuming binding to a site within the electrical field of the membrane. Second, block was ~4-fold stronger when 2 mM Ba^{2+} was the charge carrier (compared to 2 mM Ca^{2+}), suggesting ion-ion competition within the pore. Reduction of the current measured 'instantaneously' implies that Fe^{2+} equilibrates rapidly with the open pore, on the time scale of the voltage clamp (~0.1 ms). For the lowest concentration used (0.13 mM Fe^2, for experiments with Ba^{2+}), that implies binding with a bimolecular rate constant of 10^8 $M^{-1}s^{-1}$ or faster, near the diffusion limit.

Effects of Fe^{2+} on gating. The effect of Fe^{2+} on the peak current measured with the IV protocol was stronger and more voltage-dependent than with the IIV protocol. Since the current measured with the IV protocol is affected both by permeation and gating (i. e., changes in the probability that a channel is open at a particular voltage and time), this suggests that Fe^{2+} affects the response of the channel to voltage. Fig. 3 shows that the effect of Fe^{2+} can be attributed to screening and binding to surface charge. We

Molecular Pharmacology Fast Forward. Published on September 12, 2012 as DOI: 10.1124/mol.112.080184
This article has not been copyedited and formatted. The final version may differ from this version.

assumed a Guoy-Chapman-Stern for simplicity but a specific binding site on the channel can not be excluded.

Fe^{2+} permeation. In the absence of Ca^{2+}_o and Na^{+}_o $Ca_v3.1$ channels carry a significant Fe^{2+} current that saturates in the millimolar range. The currents measured in Fe^{2+} were small, showing Fe^{2+} is a poorly permeant ion, but were noticeable larger than could be attributed to gating charge movement (Fig 7B). This current increased as external Fe^{2+} was increased, suggesting that the current is carried by Fe^{2+} and not contaminating cations.

$Ca_V3.1$ as a pathway for Fe^{2+} entry. To explain the effects of Fe^{2+} on permeation we expanded a model of permeation for $Ca_v3.1$ channels to account for Fe^{2+}. The model fit the data well, although block of outward currents by 1.1 mM Fe^{2+} was underestimated (Fig. 8B). The model can assess Fe^{2+} permeation when Ca^{2+} and Mg^{2+} are present in physiological concentrations. Fig 8E and F show calculated transport rates for Fe^{2+} for external concentrations in the range of 1-10 μM and membrane potentials encountered at rest and during action potentials. $Ca_v3.1$ channels have a window current due to incomplete inactivation (Serrano et al., 1999) that leaves ~1-2% of channels open at resting membrane potentials. Because channels are open even at resting membrane potentials, we used our model of $Ca_v3.1$ channel gating to calculate the fraction of channels expected to be open in the steady state (Serrano et al., 1999). This value, times the transport rate calculated in Fig 8F, is the number of Fe^{2+} ions transported per second and channel (Fig 8D).

Comparison of Fe^{2+} to other divalent cations. We have now examined effects of several divalent cations on permeation and gating of $Ca_V3.1$: Ca^{2+}, Ba^{2+}, Mg^{2+}, Ni^{2+}, and Cd^{2+} (Khan et al., 2008; Lopin et al., 2012; Obejero-Paz et al., 2008). To a surprising extent, each ion is an individual that the channel can easily distinguish. As previously established for L-type calcium channels, there is a spectrum from highly permeant ions to strong blockers. Ca^{2+} and Ba^{2+} are the most permeant at millimolar concentrations,

Molecular Pharmacology Fast Forward. Published on September 12, 2012 as DOI: 10.1124/mol.112.080184
This article has not been copyedited and formatted. The final version may differ from this version.

although they also potently block currents carried by Na^+ at micromolar concentrations. Mg^{2+} is nearly impermeant, but blocks currents carried by Ca^{2+} from either side of the membrane (Khan et al., 2008). Fe^{2+} appears at first to be a Mg^{2+}-like blocker, but can carry small inward currents. The classical calcium channel blocker Cd^{2+} produces surprisingly large inward currents, and has a reversed voltage-dependence of channel block (Lopin et al., 2012). Ni^{2+} seems to be unique in blocking rapidly at an extracellular site (that cannot distinguish Ca^{2+} from Ba^{2+}), in addition to slow block at the selectivity filter (Obejero-Paz et al., 2008). Except for the fast block site for Ni^{2+}, these effects can be explained by a 2-site 3-barrier model as subtle quantitative changes in the energetics of ion binding, as opposed to distinct biophysical mechanisms.

Iron overload. Iron is normally tightly regulated in the body (Zhang and Enns, 2009). Increased intracellular iron has been associated with disorders in both the heart (Horwitz and Rosenthal, 1999; Kremastinos and Farmakis, 2011) and the brain (Stankiewicz and Brass, 2009), including neurological disorders such as amyotrophic lateral sclerosis (ALS), Parkinson's, and Alzheimer's disease (Oshiro et al., 2011). Intracellular iron leads to the production of reactive oxygen species that cause oxidative damage to proteins, lipids, and DNA (Giorgio et al., 2007).

Pathways for NTBI iron influx. In neurons, voltage-gated calcium channels (Gaasch et al., 2007) and NMDA receptors (Pelizzoni et al., 2011) have been implicated in NTBI. Studies with calcium channel blockers implicated both L-type channels and non-L high voltage-activated channels in Fe^{2+} entry into hippocampal neurons (Pelizzoni et al., 2011). The cerebrospinal fluid has levels of iron that saturate transferrin, leaving ~1 μM free iron (Bradbury, 1997). This iron should be maintained in its ferrous form (Fe^{2+}) by high levels of ascorbate (Bradbury 1999) and ferrireductases (Lane et al., 2010; Mills et al., 2010). In the case of cerebral hemorrage free iron levels were measured to peak at >10 μM and to remain above 5 μM for 28 days (Wan et al., 2006). This could provide sufficient free Fe^{2+} for entry into neurons via calcium channels.

Molecular Pharmacology Fast Forward. Published on September 12, 2012 as DOI: 10.1124/mol.112.080184
This article has not been copyedited and formatted. The final version may differ from this version.

The mechanism of Fe^{2+} uptake into cardiomyoctes is still debated (Chattipakorn et al., 2011). Block of L-type and T-type calcium channels in cardiomyocytes *in vivo* (Kumfu et al., 2012; Oudit et al., 2003) can decrease iron uptake into the heart, an indication that sufficient free Fe^{2+} is available in the plasma for calcium channels, and it can permeate in the presence of physiological levels of Ca^{2+}.

While the main mechanism of preventing excess iron in cells is to prevent iron uptake there are mechanisms cells use to efflux excess iron out of the cell, the main protein being ferroportin1 (Fpn1) (Donovan et al., 2000). To maintain iron homeostasis, when iron levels are increased the liver releases hepcidin (Park et al., 2001) which binds to Fpn1 causing its endocytosis and degradation (Nemeth et al., 2004). Normally this reduces plasma iron levels by decreasing Fpn1 in intestinal cells, decreasing iron absorption from the diet (Ganz, 2011). In iron overload conditions where iron absorption is unregulated in this way due to repeated transfusions to treat a blood disorder the mechanism of hepicin downregulating Fpn1 could cause iron handling problems. In cells with unregulated Fe^{2+} entry, such as cardiomyocytes and neurons which have a large number of calcium channels, hepcidin release will cause Fpn1 to decrease (Wang et al., 2010), lowering the capacity of cells to export Fe^{2+} while calcium channels continue to allow unregulated Fe^{2+} entry.

Our results indicate that $Ca_v3.1$ channels can constitute a pathway for iron entry at resting membrane potentials, and possibly during the course of action potentials, when extracellular Fe^{2+} reaches concentrations in the micromolar range.

Molecular Pharmacology Fast Forward. Published on September 12, 2012 as DOI: 10.1124/mol.112.080184
This article has not been copyedited and formatted. The final version may differ from this version.

Acknowledgements

We thank Dr. Ed Perez-Reyes (U. Virginia) for the HEK 293 cell line stably transfected with $Ca_V3.1$.

Molecular Pharmacology Fast Forward. Published on September 12, 2012 as DOI: 10.1124/mol.112.080184
This article has not been copyedited and formatted. The final version may differ from this version.

Authorship Contributions

Participated in research design: Lopin, Obejero-Paz, Thévenod, Jones

Conducted experiments: Lopin, Gray, Obejero-Paz, Thevenod

Contributed new reagents or analytical tools: none

Performed data analysis: Lopin, Obejero-Paz, Thévenod, Jones

Wrote or contributed to the writing of the manuscript: Lopin, Obejero-Paz, Thévenod, Jones

Molecular Pharmacology Fast Forward. Published on September 12, 2012 as DOI: 10.1124/mol.112.080184
This article has not been copyedited and formatted. The final version may differ from this version.

References

Almers W and McCleskey EW (1984) Non-selective conductance in calcium channels of frog muscle: calcium selectivity in a single-file pore. *J Physiol (Lond)* **353**: 585-608.

Anderson GJ and Vulpe CD (2009) Mammalian iron transport. *Cell Mol Life Sci* **66**(20): 3241-3261.

Andrews NC (1999) Disorders of iron metabolism. *N Engl J Med* **341**(26): 1986-1995.

Beedle AM, Hamid J and Zamponi GW (2002) Inhibition of transiently expressed low- and high-voltage-activated calcium channels by trivalent metal cations. *J MembrBiol* **187**(3): 225-238.

Bradbury MW (1997) Transport of iron in the blood-brain-cerebrospinal fluid system. *J Neurochem* **69**(2): 443-454.

Chattipakorn N, Kumfu S, Fucharoen S and Chattipakorn S (2011) Calcium channels and iron uptake into the heart. *World J Cardiol* **3**(7): 215-218.

Clark P, Britton LJ and Powell LW (2010) The diagnosis and management of hereditary haemochromatosis. *Clin Biochem Rev* **31**(1): 3-8.

Donovan A, Brownlie A, Zhou Y, Shepard J, Pratt SJ, Moynihan J, Paw BH, Drejer A, Barut B, Zapata A, Law TC, Brugnara C, Lux SE, Pinkus GS, Pinkus JL, Kingsley PD, Palis J, Fleming MD, Andrews NC and Zon LI (2000) Positional cloning of zebrafish ferroportin1 identifies a conserved vertebrate iron exporter. *Nature* **403**(6771): 776-781.

Dorey C, Cooper C, Dickson DP, Gibson JF, Simpson RJ and Peters TJ (1993) Iron speciation at physiological pH in media containing ascorbate and oxygen. *Br J Nutr* **70**(1): 157-169.

Elinder F and Arhem P (2003) Metal ion effects on ion channel gating. *Q Rev Biophys* **36**(4): 373-427.

Gaasch JA, Geldenhuys WJ, Lockman PR, Allen DD and Van der Schyf CJ (2007) Voltage-gated calcium channels provide an alternate route for iron uptake in neuronal cell cultures. *Neurochem Res* **32**: 1686-1693.

Ganz T (2011) Hepcidin and iron regulation, 10 years later. *Blood* **117**(17): 4425-4433.

Garrick MD, Kuo HC, Vargas F, Singleton S, Zhao L, Smith JJ, Paradkar P, Roth JA and Garrick LM (2006) Comparison of mammalian cell lines expressing distinct isoforms of divalent metal transporter 1 in a tetracycline-regulated fashion. *Biochem J* **398**(3): 539-546.

Giorgio M, Trinei M, Migliaccio E and Pelicci PG (2007) Hydrogen peroxide: a metabolic by-product or a common mediator of ageing signals? *Nat Rev Mol Cell Biol* **8**(9): 722-728.

Hering J, Feltz A and Lambert RC (2004) Slow inactivation of the $Ca_V3.1$ isotype of T-type calcium channels. *J Physiol (Lond)* **555**: 331-334.

Hess P and Tsien RW (1984) Mechanism of ion permeation through calcium channels. *Nature* **309**(5967): 453-456.

Hodgkin AL and Huxley AF (1952) The components of membrane conductance in the giant axon of *Loligo*. *J Physiol (Lond)* **116**: 473-496.

Horwitz LD and Rosenthal EA (1999) Iron-mediated cardiovascular injury. *Vasc Med* **4**(2): 93-99.

Huang L, Keyser BM, Tagmose TM, Hansen JB, Taylor JT, Zhuang H, Zhang M, Ragsdale DS and Li M (2004) NNC 55-0396 [(1S,2S)-2-(2-(N-[(3-benzimidazol-2-yl)propyl]-N-methylamino)ethyl)-6-fluoro-1,2,3,4-tetrahydro-1-isopropyl-2-naphtyl cyclopropanecarboxylate dihydrochloride]: A new selective inhibitor of T-type calcium channels *J Pharmacol Exp Ther* **309**: 193-199.

Iancu TC, Shiloh H, Link G, Bauminger ER, Pinson A and Hershko C (1987) Ultrastructural pathology of iron-loaded rat myocardial cells in culture. *Br J Exp Pathol* **68**(1): 53-65.

Kang HW, Park JY, Jeong SW, Kim JA, Moon HJ, Perez-Reyes E and Lee JH (2005) A molecular determinant of nickel inhibition in $Ca_V3.2$ T-type calcium channels. *J Biol Chem* **281**: 4823-4830.

Khan N, Gray IP, Obejero-Paz CA and Jones SW (2008) Permeation and gating in $Ca_V3.1$ (α1G) T-type calcium channels. Effects of Ca^{2+}, Ba^{2+}, Mg^{2+}, and Na^{+}. *J Gen Physiol* **132**(2): 223-238.

Kim E, Giri SN and Pessah IN (1995) Iron(Ii) Is a Modulator of Ryanodine-Sensitive Calcium Channels of Cardiac-Muscle Sarcoplasmic-Reticulum. *Toxicol Appl Pharm* **130**(1): 57-66.

Kremastinos DT and Farmakis D (2011) Iron overload cardiomyopathy in clinical practice. *Circulation* **124**: 2253-2263.

Kumfu S, Chattipakorn S, Chinda K, Fucharoen S and Chattipakorn N (2012) T-type calcium channel blockade improves survival and cardiovascular function in thalassemic mice. *Eur J Haematol* **88**(6): 535-548.

Kumfu S, Chattipakorn S, Srichairatanakool S, Settakorn J, Fucharoen S and Chattipakorn N (2011) T-type calcium channel as a portal of iron uptake into cardiomyocytes of beta-thalassemic mice. *Eur J Haematol* **86**(2): 156-166.

Kuryshev YA, Brittenham GM, Fujioka H, Kannan P, Shieh CC, Cohen SA and Brown AM (1999) Decreased sodium and increased transient outward potassium currents in iron-loaded cardiac myocytes. Implications for the arrhythmogenesis of human siderotic heart disease. *Circulation* **100**(6): 675-683.

Kwiatkowski JL (2011) Management of transfusional iron overload - differential properties and efficacy of iron chelating agents. *J Blood Med* **2**: 135-149.

Lane DJ, Robinson SR, Czerwinska H, Bishop GM and Lawen A (2010) Two routes of iron accumulation in astrocytes: ascorbate-dependent ferrous iron uptake via the divalent metal transporter (DMT1) plus an independent route for ferric iron. *Biochem J* **432**(1): 123-132.

Liuzzi JP, Aydemir F, Nam H, Knutson MD and Cousins RJ (2006) Zip14 (Slc39a14) mediates non-transferrin-bound iron uptake into cells. *Proc Natl Acad Sci U S A* **103**(37): 13612-13617.

Lopin KV, Obejero-Paz CA and Jones SW (2010) Evaluation of a two-site, three-barrier model for permeation in $Ca_V3.1$ (α1G) T-type calcium channels: Ca^{2+}, Ba^{2+}, Mg^{2+}, and Na^{+}. *J Membr Biol* **235**(2): 131-143.

Lopin KV, Thévenod F, Page JC and Jones SW (2012) Cd^{2+} block and permeation in $Ca_V3.1$ (α1G) T-type calcium channels. A candidate mechanism for Cd^{2+} influx. *Molecular Pharmacology, submitted*.

Loreal O, Gosriwatana I, Guyader D, Porter J, Brissot P and Hider RC (2000) Determination of non-transferrin-bound iron in genetic hemochromatosis using a new HPLC-based method. *J Hepatol* **32**(5): 727-733.

Mills E, Dong XP, Wang F and Xu H (2010) Mechanisms of brain iron transport: insight into neurodegeneration and CNS disorders. *Future Med Chem* **2**(1): 51-64.

Mwanjewe J and Grover AK (2004) Role of transient receptor potential canonical 6 (TRPC6) in non-transferrin-bound iron uptake in neuronal phenotype PC12 cells. *Biochem J* **378**(Pt 3): 975-982.

Nemeth E, Tuttle MS, Powelson J, Vaughn MB, Donovan A, Ward DM, Ganz T and Kaplan J (2004) Hepcidin regulates cellular iron efflux by binding to ferroportin and inducing its internalization. *Science* **306**(5704): 2090-2093.

Obejero-Paz CA, Gray IP and Jones SW (2008) Ni^{2+} block of CaV3.1 (α1G) T-type calcium channels. *J Gen Physiol* **132**(2): 239-250.

Oshiro S, Morioka MS and Kikuchi M (2011) Dysregulation of iron metabolism in Alzheimer's disease, Parkinson's disease, and amyotrophic lateral sclerosis. *Adv Pharmacol Sci* **2011**: 378278.

Oudit GY, Sun H, Trivieri MG, Koch SE, Dawood F, Ackerley C, Yazdanpanah M, Wilson GJ, Schwartz A, Liu PP and Backx PH (2003) L-type Ca^{2+} channels provide a major pathway for iron entry into cardiomyocytes in iron-overload cardiomyopathy. *Nat Med* **9**(9): 1187-1194.

Park CH, Valore EV, Waring AJ and Ganz T (2001) Hepcidin, a urinary antimicrobial peptide synthesized in the liver. *J Biol Chem* **276**(11): 7806-7810.

Parkes JG, Liu Y, Sirna JB and Templeton DM (2000) Changes in gene expression with iron loading and chelation in cardiac myocytes and non-myocytic fibroblasts. *J Mol Cell Cardiol* **32**(2): 233-246.

Pelizzoni I, Macco R, Morini MF, Zacchetti D, Grohovaz F and Codazzi F (2011) Iron handling in hippocampal neurons: activity-dependent iron entry and mitochondria-mediated neurotoxicity. *Aging Cell* **10**(1): 172-183.

Perez-Reyes E (2003) Molecular physiology of low-voltage-activated T-type calcium channels. *Physiol Rev* **83**(1): 117-161.

Rodman DM, Reese K, Harral J, Fouty B, Wu S, West J, Hoedt-Miller M, Tada Y, Li KX, Cool C, Fagan K and Cribbs L (2005) Low-voltage-activated (T-type) calcium channels control proliferation of human pulmonary artery myocytes. *Circ Res* **96**: 864-872.

Serrano JR, Dashti SR, Perez-Reyes E and Jones SW (2000) Mg^{2+} block unmasks Ca^{2+}/Ba^{2+} selectivity of α1G T-type calcium channels. *Biophys J* **79**(6): 3052-3062.

Serrano JR, Perez-Reyes E and Jones SW (1999) State-dependent inactivation of the α1G T-type calcium channel. *J Gen Physiol* **114**(2): 185-201.

Stankiewicz JM and Brass SD (2009) Role of iron in neurotoxicity: a cause for concern in the elderly? *Curr Opin Clin Nutr Metab Care* **12**(1): 22-29.

Traboulsie A, Chemin J, Chevalier M, Quignard JF, Nargeot J and Lory P (2007) Subunit-specific modulation of T-type calcium channels by zinc. *J Physiol* **578**(Pt 1): 159-171.

Tsushima RG, Wickenden AD, Bouchard RA, Oudit GY, Liu PP and Backx PH (1999) Modulation of iron uptake in heart by L-type Ca^{2+} channel modifiers: possible implications in iron overload. *Circ Res* **84**(11): 1302-1309.

Viollier E, Inglett PW, Hunter K, Roychoudhury AN and Van Cappellen P (2000) The ferrozine method revisited: Fe(II)/Fe(III) determination in natural waters. *Appl Geochem* **15**(6): 785-790.

Wan S, Hua Y, Keep RF, Hoff JT and Xi G (2006) Deferoxamine reduces CSF free iron levels following intracerebral hemorrhage. *Acta Neurochir Suppl* **96**: 199-202.

Wang SM, Fu LJ, Duan XL, Crooks DR, Yu P, Qian ZM, Di XJ, Li J, Rouault TA and Chang YZ (2010) Role of hepcidin in murine brain iron metabolism. *Cell Mol Life Sci* **67**(1): 123-133.

Winegar BD, Kelly R and Lansman JB (1991) Block of current through single calcium channels by Fe, Co, and Ni. Location of the transition metal binding site in the pore. *J Gen Physiol* **97**(2): 351-367.

Woodhull AM (1973) Ionic blockage of sodium channels in nerve. *J Gen Physiol* **61**: 687-708.

Yunker AMR and McEnery MW (2003) Low voltage-activated ("T-type") calcium channels in review. *J Bioenerg Biomembr* **35**: 533-575.

Zhang AS and Enns CA (2009) Molecular mechanisms of normal iron homeostasis. *Hematology Am Soc Hematol Educ Program*: 207-214.

Molecular Pharmacology Fast Forward. Published on September 12, 2012 as DOI: 10.1124/mol.112.080184
This article has not been copyedited and formatted. The final version may differ from this version.

Zhou W and Jones SW (1995) Surface charge and calcium channel saturation in bullfrog sympathetic neurons. *J Gen Physiol* **105**(4): 441-462.

Footnotes

This study was supported by the National Institutes of Health, National Institute of Neurological Diseases and Stroke [NS24471], and FT Deutsche Forschungsgemeinschaft [TH345/11-1] and Stiftung Westermann-Westdorp.

Correspondence to Stephen W. Jones, Department of Physiology and Biophysics, Case Western Reserve University, Cleveland, OH 44106.

Current affiliation of Carlos A. Obejero-Paz: ChanTest Corporation, Cleveland, OH 44128.

Molecular Pharmacology Fast Forward. Published on September 12, 2012 as DOI: 10.1124/mol.112.080184
This article has not been copyedited and formatted. The final version may differ from this version.

Figure Legends

Fig. 1. Block by Fe^{2+} of currents carried by Ca^{2+} with the IIV protocol. A, sample records of currents, using the protocol illustrated below the middle record, in control (left), after addition of Fe^{2+} (middle), and after washout of Fe^{2+} (right). 3 kHz Gaussian filter. Currents shown here are in 40 mV increments. B, IIV relations from the protocol of A, in control (0 Fe^{2+}), and in two concentrations of Fe^{2+} (n=4 for each concentration). C, expanded view of IIV relations. D, chord conductances calculated for the data from B. E, Inhibition by Fe^{2+}, expressed as the ratio of the chord conductance in Fe^{2+} to the chord conductance in control conditions. Data not shown near the reversal potential, where errors in calculating conductances can be large. Solid curves are fits to a Woodhull (1973) model. Symbols in B apply to panels B-E.

Fig. 2. Block by Fe^{2+} of currents carried by Ca^{2+} using the IV protocol. A, sample records, shown in 20 mV increments, with 3 kHz Gaussian filter. B, IV relations from the protocol of A, for the same cells as Fig. 1. C, IV relations on an expanded scale. D, chord conductances from the data of B. E, inhibition by Fe^{2+}, as the chord conductance ratio, fitted to a Woodhull (1973) model. Data not shown near the reversal potential. Symbols in B apply to panels B-E.

Fig. 3. Effects of Fe^{2+} on gating. A, effect of Fe^{2+} on the time-to-peak of currents, using the IV protocol. B, effect of Fe^{2+} on the time constant for deactivation, using the IIV protocol. C, effect of Fe^{2+} on channel activation, as the ratio of the peak IV current to the IIV current at the same voltage. D, voltage shifts for the data shown in A-C, for the activation curve ($\Delta P_{O,r}$), for deactivation ($\Delta\tau_{IIV}$), and for time to peak (Δt_{Peak}). The solid curve is a fit to Gouy-Chapman-Stern theory. The dashed curve is the fit to voltage shifts

Molecular Pharmacology Fast Forward. Published on September 12, 2012 as DOI: 10.1124/mol.112.080184
This article has not been copyedited and formatted. The final version may differ from this version.

induced by Ca^{2+}, Ba^{2+}, and Mg^{2+}, from Khan et al. (2008). Symbols in A apply to panels A-C. Data not shown near the reversal potential in A-C. Same cells as Figs. 1-2.

Fig. 4. Effects of Fe^{2+} with 2 mM Ba^{2+} as charge carrier. A, sample records with the IIV protocol, 40 mV increments. B, sample records with the IV protocol, 20 mV increments. 3 kHz Gaussian filter.

Fig. 5. Analysis of effects of Fe^{2+} in 2 mM Ba^{2+}. A, IIV relations in control and in 0.13 mM Fe^{2+}. B, inhibition by Fe^{2+}, from the ratio of chord conductances (Fe^{2+}/control), fitted to a Woodhull (1973) model. C, IV relations (currents from +50 to +100 mV not shown). D, activation curves, from IV/IIV current ratios. Data not shown near the reversal potential in B and D. n=4 for all panels.

Fig. 6. Permeation by Fe^{2+}. A, sample records with the IIV protocol, in 40 mV increments, with 3 kHz Gaussian filter. The inset below the middle record shows currents from -100 to +20 mV, on a 5-fold expanded scale. B, IIV relations. C, IIV relations on an expanded scale. Symbols in C also apply to B. Data in B-C are from 7 cells, 4 in 1.1 mM Fe^{2+}, 5 in 8.9 mM Fe^{2+}.

Fig. 7. Comparison of tail currents in Fe^{2+} to gating currents. A, sample records with the IIV protocol, in 40 mV increments. Note partial recovery (right panel) following superfusion with the solution used to isolate gating currents (La^{3+} + Cd^{2+}). The insets below the middle two records are on a 5× expanded scale, to show tail currents in Fe^{2+} and on- and off gating currents in La^{3+} + Cd^{2+}. 3 kHz Gaussian filter. B, integrated tail currents in Fe^{2+} compared to Q_{on} (measured during depolarization to +60 mV) and Q_{off} (measured following repolarization). n=5 (Fe^{2+} tails) and n=4 (Q_{on} and Q_{off}). C, the portion of the integrated tail current amplitude attributable to Fe^{2+} entry, as a function of

Molecular Pharmacology Fast Forward. Published on September 12, 2012 as DOI: 10.1124/mol.112.080184
This article has not been copyedited and formatted. The final version may differ from this version.

Fe^{2+}, for the 5 cells in B, and 2 cells tested at ~1 mM Fe^{2+}. The solid curve is a fit to a single saturable binding site with K_D = 4.7 mM and maximal Q = 0.78 pC.

Fig. 8. A 2S3B Eyring model for permeation and block by Fe^{2+}. A, energy levels and electrical distances for barriers and wells, for Ca^{2+} and Fe^{2+}. Energy levels (outside to inside) were 9.32, -12.73, 5.26, -6.97, and 15.65 RT. The electical distances and energy profiles for Na^{+}, Mg^{2+}, and Ba^{2+} are from Lopin et al. (2011). B to D, fits of the model to experimental IIV data are shown for permeation (B), block of current carried by 2 mM Ca^{2+} (C), and block with 2 mM Ba^{2+} (C). E, calculation of the rate of Fe^{2+} entry for the indicated Fe^{2+}_o concentrations, in the presence of 2 mM Ca^{2+}_o, for a single open channel. F, calculation of the steady-state rate of Fe^{2+} entry considering channel gating (activation and inactivation). The steady-state P_O-V relationship calculated from the Serrano et al. (1999) model was convolved with the curves in panel E.

Figure 1

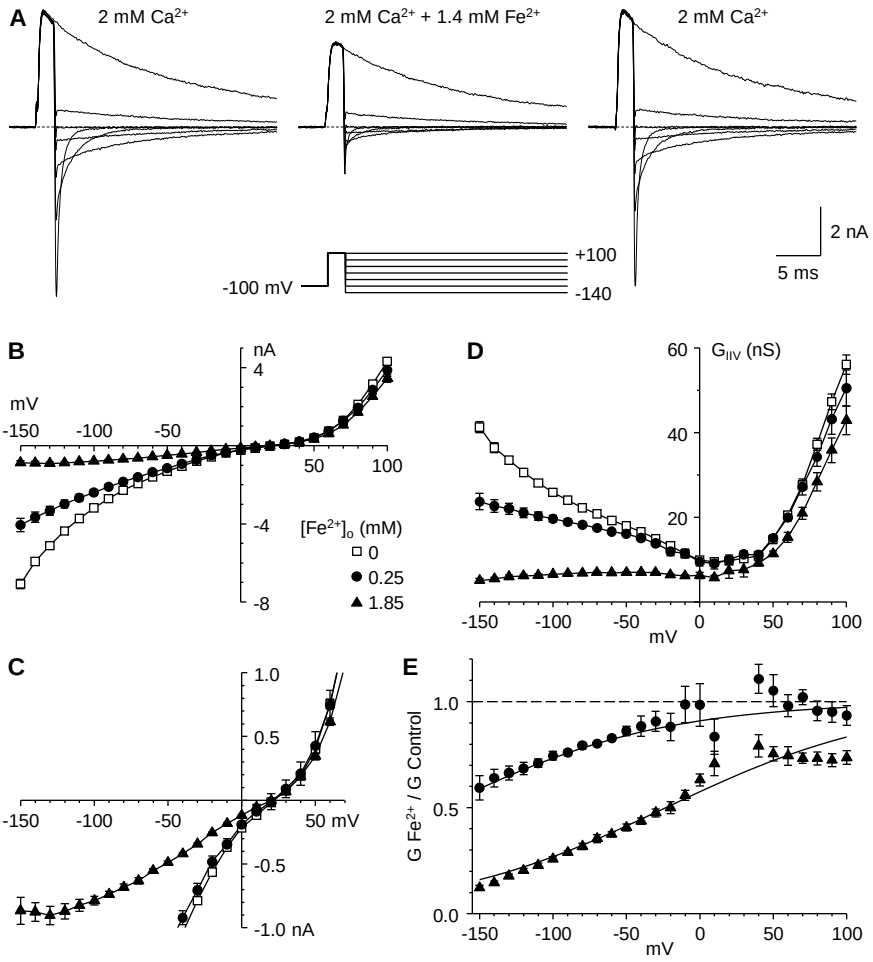
A
2 mM Ca2+
2 mM Ca2+ + 1.4 mM Fe2+
2 mM Ca2+
-100 mV
+100
-140
2 nA
5 ms
B
nA
4
mV
-150
-100
-50
50
100
-4
-8
[Fe2+]o (mM)
0
0.25
1.85
D
60
GIIV (nS)
40
20
-150
-100
-50
0
50
100
mV
C
1.0
0.5
-150
-100
-50
50 mV
-0.5
-1.0 nA
E
1.0
0.5
0.0
G Fe2+ / G Control
-150
-100
-50
0
50
100
mV

Figure 2

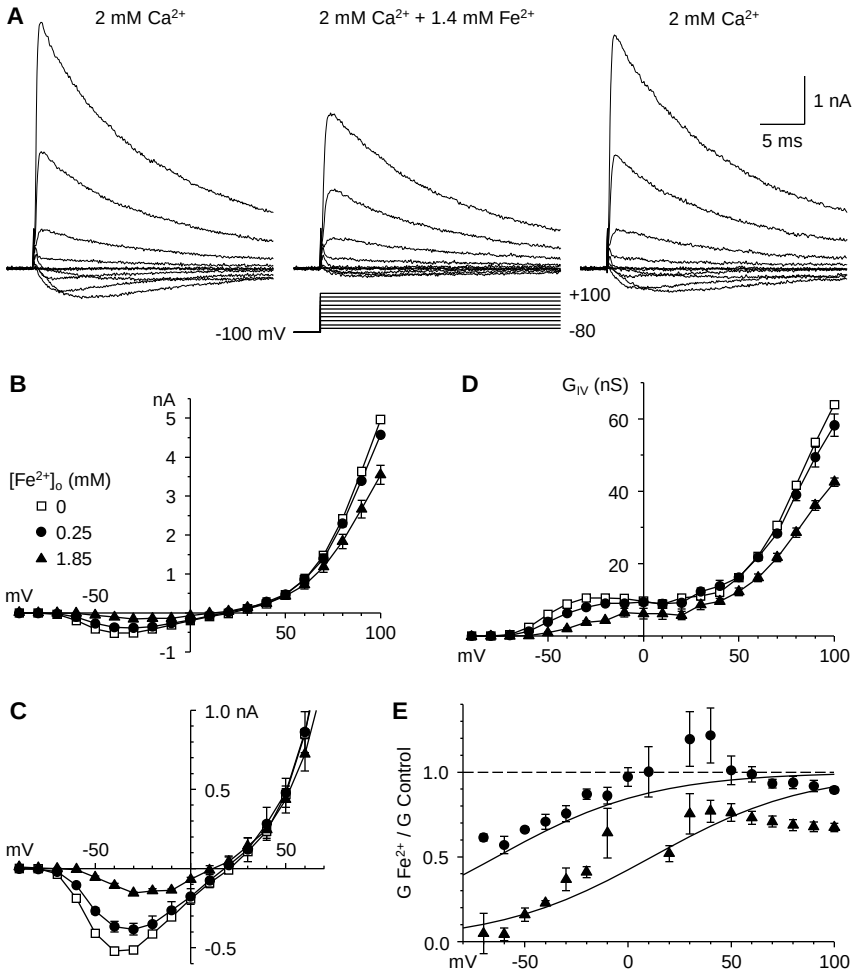
A
2 mM Ca2+
2 mM Ca2+ + 1.4 mM Fe2+
2 mM Ca2+
1 nA
5 ms
+100
-80
-100 mV
B
nA
[Fe2+]o (mM)
0
0.25
1.85
mV
-50
50
100
D
GIV (nS)
60
40
20
C
1.0 nA
0.5
-0.5
E
G Fe2+ / G Control
1.0
0.5
0.0

Figure 3

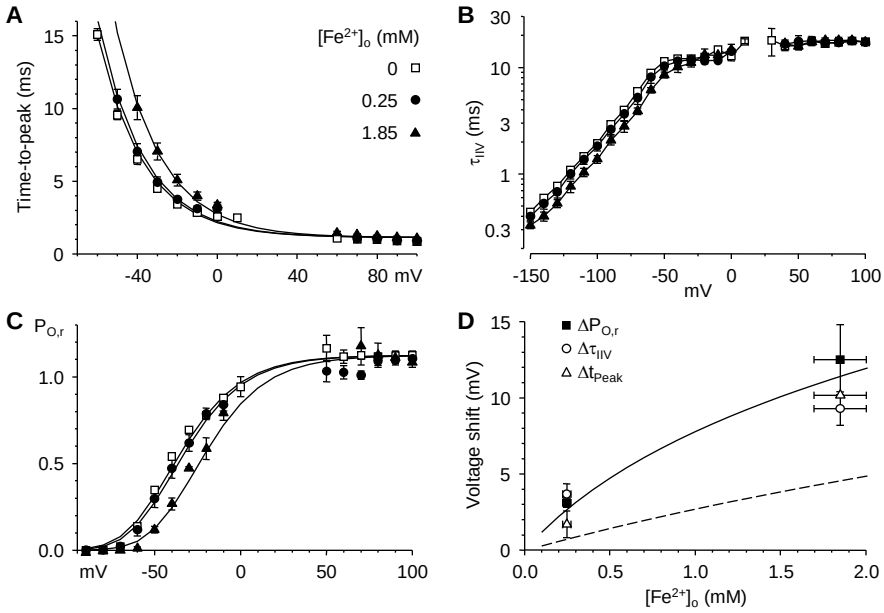
A
Time-to-peak (ms)
15
10
5
0
-40
0
40
80 mV
[Fe2+]o (mM)
0
0.25
1.85
B
τIIV (ms)
30
10
3
1
0.3
-150
-100
-50
0
50
100
mV
C
PO,r
1.0
0.5
0.0
mV
-50
0
50
100
D
Voltage shift (mV)
15
10
5
0
0.0
0.5
1.0
1.5
2.0
[Fe2+]o (mM)
ΔPO,r
ΔτIIV
ΔtPeak

Figure 4

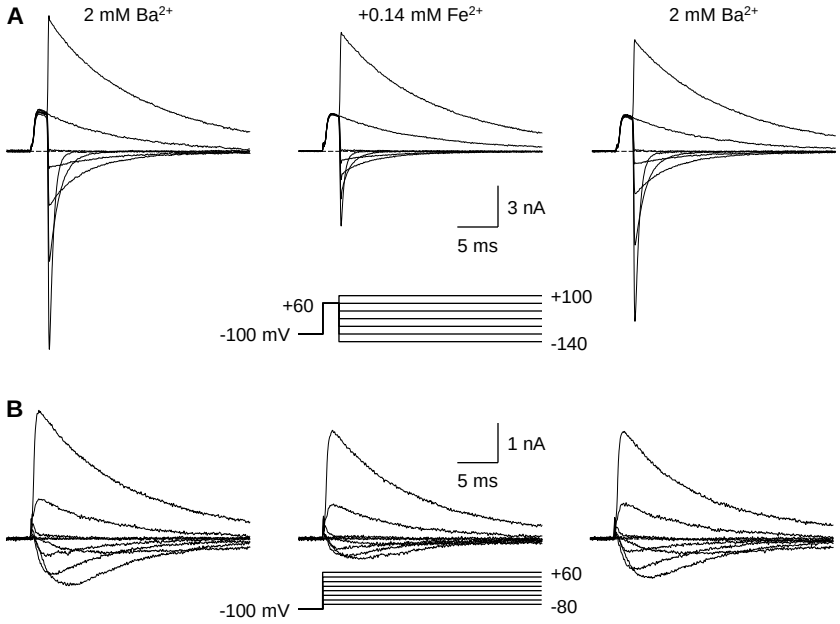
A
2 mM Ba2+
+0.14 mM Fe2+
2 mM Ba2+
3 nA
5 ms
+60
-100 mV
+100
-140
B
1 nA
5 ms
-100 mV
+60
-80

Figure 5

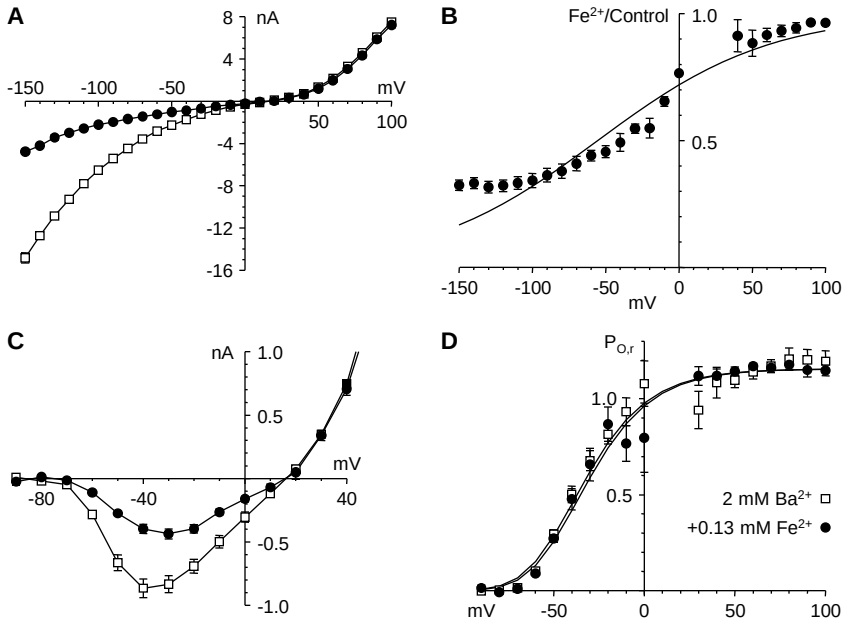
A
nA
8
4
-4
-8
-12
-16
-150
-100
-50
50
100
mV
B
Fe2+/Control
1.0
0.5
-150
-100
-50
0
50
100
mV
C
nA
1.0
0.5
-0.5
-1.0
-80
-40
40
mV
D
PO,r
1.0
0.5
2 mM Ba2+
+0.13 mM Fe2+
mV
-50
0
50
100

Figure 6

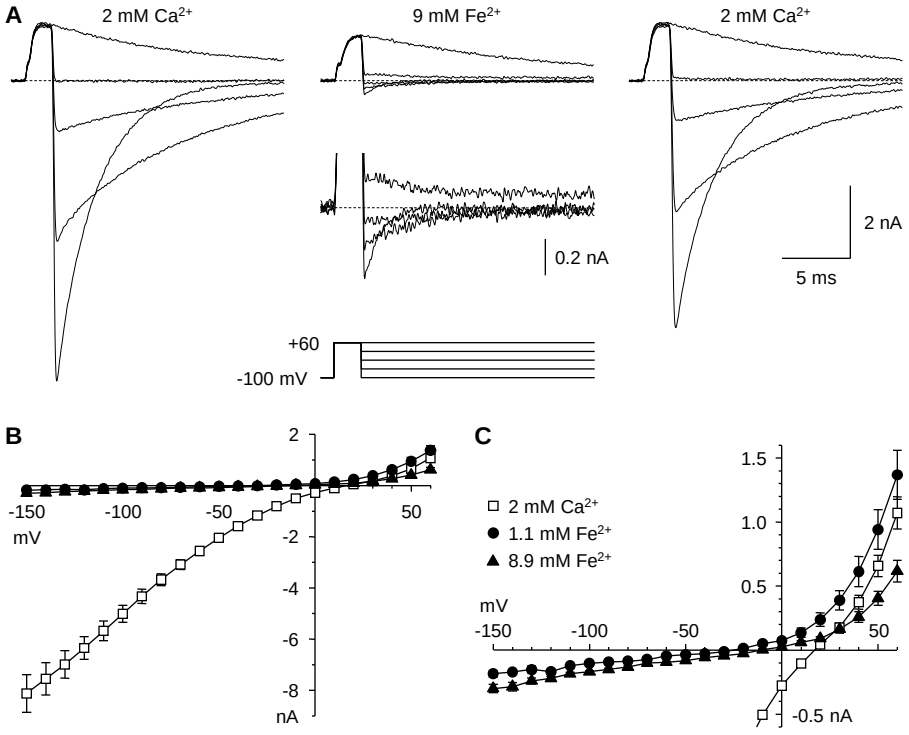
A
2 mM Ca2+
9 mM Fe2+
2 mM Ca2+
0.2 nA
2 nA
5 ms
+60
-100 mV
B
2
-150
-100
-50
50
mV
-2
-4
-6
-8
nA
C
2 mM Ca2+
1.1 mM Fe2+
8.9 mM Fe2+
1.5
1.0
0.5
mV
-150
-100
-50
50
-0.5 nA

Figure 7

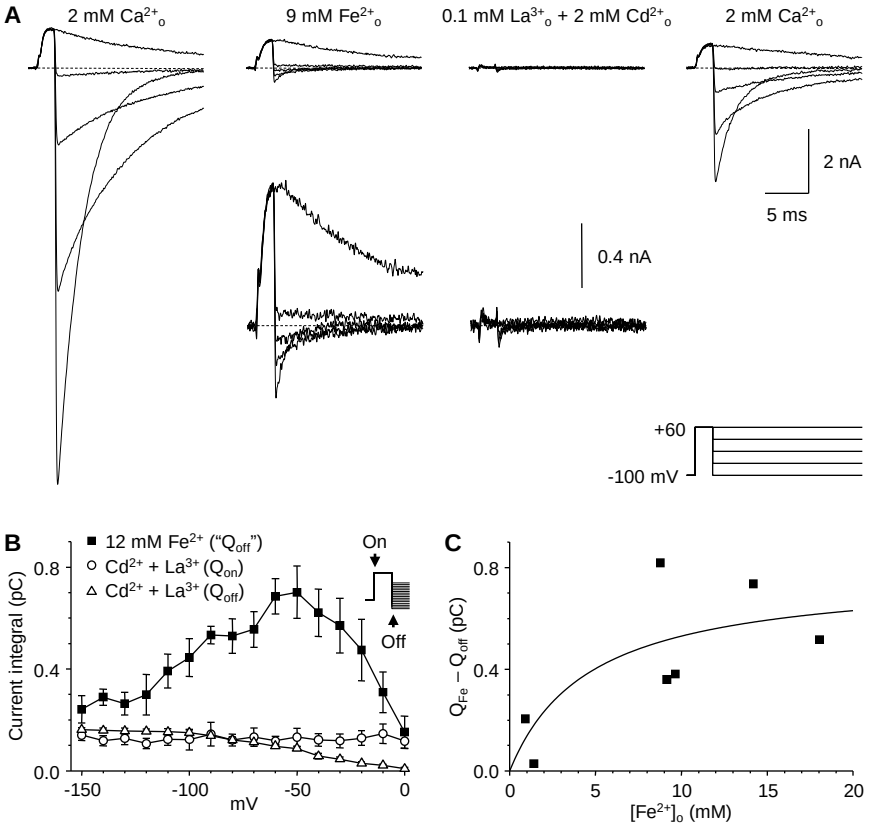
A
2 mM Ca2+o
9 mM Fe2+o
0.1 mM La3+o + 2 mM Cd2+o
2 mM Ca2+o
2 nA
5 ms
0.4 nA
+60
-100 mV
B
12 mM Fe2+ ("Qoff")
Cd2+ + La3+ (Qon)
Cd2+ + La3+ (Qoff)
On
Off
Current integral (pC)
0.8
0.4
0.0
-150
-100
-50
0
mV
C
QFe – Qoff (pC)
0.8
0.4
0.0
0
5
10
15
20
[Fe2+]o (mM)

Figure 8

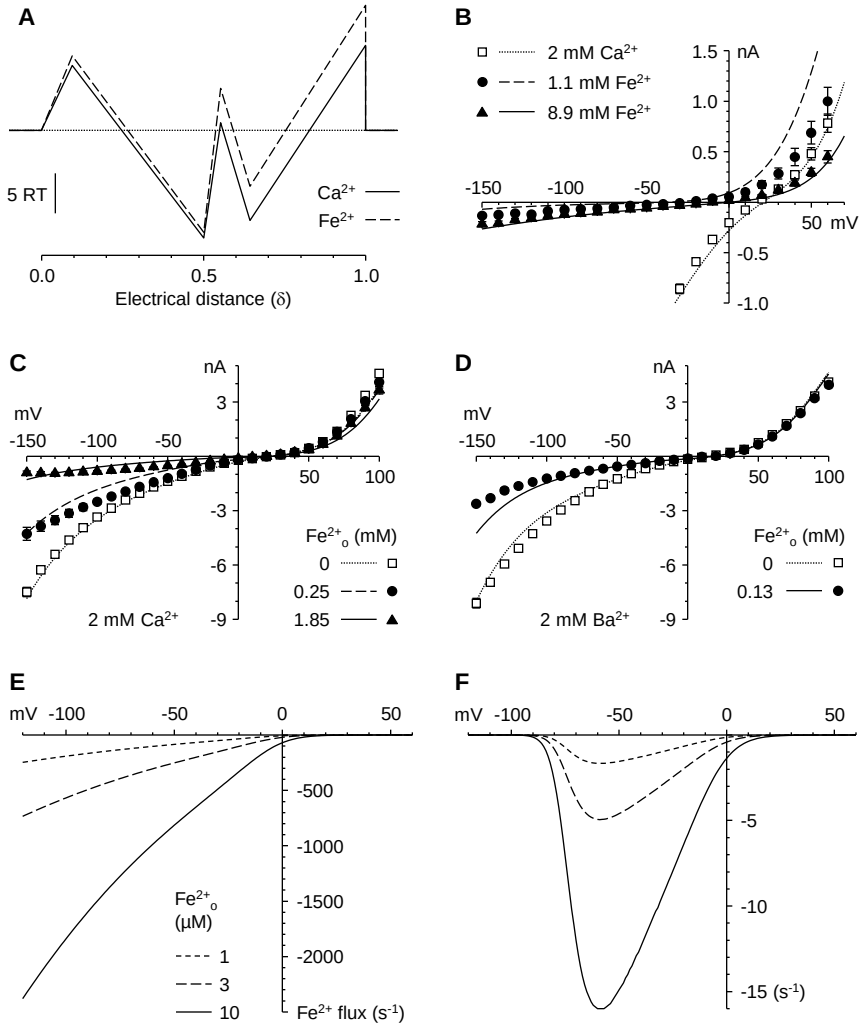
A
5 RT
Ca2+
Fe2+
0.0
0.5
1.0
Electrical distance (δ)
B
2 mM Ca2+
1.1 mM Fe2+
8.9 mM Fe2+
nA
1.5
1.0
0.5
-0.5
-1.0
-150
-100
-50
50 mV
C
nA
mV
-150
-100
-50
50
100
3
-3
-6
-9
Fe2+o (mM)
0
0.25
1.85
2 mM Ca2+
D
nA
mV
-150
-100
-50
50
100
3
-3
-6
-9
Fe2+o (mM)
0
0.13
2 mM Ba2+
E
mV -100
-50
0
50
-500
-1000
-1500
-2000
Fe2+o (μM)
1
3
10
Fe2+ flux (s-1)
F
mV -100
-50
0
50
-5
-10
-15 (s-1)